symmetry

MDPI

Article

Revisiting the Two-Dimensional Hydrogen Atom: Azimuthal Wavefunctions for Illustrating *s*, *p*, *d*, and *f* Orbitals

Phatlada Sathongpaen [1], Suphawich Jindanate [1] and Attapon Amthong [1,2,*]

[1] Department of Physics, Faculty of Science, Naresuan University, Phitsanulok 65000, Thailand; phatladas64@nu.ac.th (P.S.); suphawichj65@nu.ac.th (S.J.)
[2] Research Center for Academic Excellence in Applied Physics, Naresuan University, Phitsanulok 65000, Thailand
* Correspondence: attapona@nu.ac.th

Abstract: The two-dimensional (2D) hydrogen atom is a fundamental atomic model that is important for various technologies based on 2D materials. Here, the atomic model is revisited to enhance understanding of the hydrogen wavefunctions. Unlike in previous studies, we propose an alternative expression of azimuthal wavefunctions, which are the eigenstates of the square of angular momentum and exhibit rotational symmetry. Remarkably, our expression leads to the rotation and oscillation along the azimuthal direction of the probability densities, which do not appear in the conventional wavefunctions. These behaviors are validated by the numerical results obtained through the 2D finite difference approach. Variation in oscillator strengths due to the rotation of wavefunctions is observed in our proposed 2D hydrogen wavefunctions, whereas those due to the conventional wavefunctions remain constant. More importantly, the proposed wavefunctions' advantage is illustrating the orbital shapes of the planar hydrogen states, whose orientation is labeled here using Cartesian representation for the first time. This study can be applied to visualize the orbital characteristics of the states in quantum confinement with a radial potential.

Keywords: square of angular momentum; oscillator strength; atomic orbitals; *spdf* notation

check for updates

Citation: Sathongpaen, P.; Jindanate, S.; Amthong, A. Revisiting the Two-Dimensional Hydrogen Atom: Azimuthal Wavefunctions for Illustrating *s*, *p*, *d*, and *f* Orbitals. *Symmetry* **2024**, *16*, 1163. https://doi.org/10.3390/sym16091163

Academic Editors: Xing-Gang Wu and Aurélien Drezet

Received: 26 July 2024
Revised: 30 August 2024
Accepted: 3 September 2024
Published: 5 September 2024

1. Introduction

According to recent growing interest in the low-dimensional systems of single-layer and thin materials [1–3], the atomic model of the 2D hydrogen atom has gained significant importance as a foundational concept. It can be applied to describe donor atoms and excitons in thin semiconductors [4–7], both of which play a key role in various fields of science and technology. In quantum computing [8–10], individual donor atoms within a semiconductor can serve as qubits for quantum information processing. In single-electron transistors [11–13], donor atoms significantly influence the current–voltage characteristics of atomic devices. In 2D semiconductors [14–16], excitons bound by strong Coulomb interaction determine optical properties such as selection rules, circular dichroism, and efficient recombination. Therefore, the atomic model of the 2D hydrogen atom undoubtedly provides insight into and facilitates understanding of these technologies.

The theoretical framework regarding the 2D hydrogen atom has remained a subject of ongoing attention and further development for many decades [17–19]. It was first studied in 1967 by Zaslow and Zandler [20], who successfully solved the Schrödinger equation to obtain the exact eigenvalues and eigenfunctions of the 2D hydrogen atom. This planar atomic model has been revisited by Yang et al. [21], who conducted further investigations into the dipole matrix elements, Stark effect, optical transitions, and fine structures. Subsequently, the 2D hydrogen atom in various confinement potentials was investigated [22–24]. Stevanovic and Sen found that incidental degeneracy of the confined hydrogen states occurs at a particular radius of the infinite circular potential [22]. In the presence of a magnetic field and an electric field, the 2D hydrogen atom is explored numerically and analytically [25–31]. The explorations

revealed that a tilted magnetic field can be used to manipulate the density of the hydrogen states [32]. The field also causes strong anisotropic distribution of the probability densities of the hydrogen states [33]. Meanwhile, an electric field leads to a decrease in the binding energy of the ground state and an increase in the oscillator strength of the 2D hydrogen atom [34]. Additionally, the effect of spin–orbit coupling on a 2D hydrogen atom has been reported; a large spin–orbit interaction results in the splitting of energy levels and the tight binding of an electron [35,36]. It is worth recognizing that the azimuthal wave function used in these previous studies is complex. Because it consists of real and imaginary components, plotting the complex wavefunction to visualize and understand the orbital shapes of the 2D hydrogen states is a struggle.

This work revisits the two-dimensional hydrogen atom. First, the planar hydrogen wavefunctions are investigated numerically using the 2D finite difference method. Surprisingly, the numerical results show that the spatial distribution of the probability densities (PDs) of most hydrogen states fluctuates along the azimuthal direction. This behavior has not been seen before in PDs due to the conventional analytical wavefunctions. Consequently, the new derivation of alternative azimuthal wavefunctions is presented here. Our proposed wavefunctions are confirmed by the excellent agreement with the numerical wavefunctions. The oscillator strength due to the proposed hydrogen wavefunctions is also explored and compared with the conventional wavefunctions. Moreover, our expression of the planar hydrogen states yields real-valued functions. These functions enable straightforward visualization of the orbital shapes and orientation, facilitating the first-ever labeling of s, p, d, and f orbitals of the 2D hydrogen states using Cartesian representation.

2. Theoretical and Numerical Calculations

In the problem of the 2D hydrogen atom, the Schrödinger equation describing an electron trapped in a coulomb potential is given by

$$-\frac{\hbar^2}{2m_e}\nabla^2\Psi(r,\phi) - \frac{e^2}{4\pi\varepsilon_0 r}\Psi(r,\phi) = E\Psi(r,\phi) \tag{1}$$

where m_e is the electron mass, e is the electron charge, and ε_0 is the vacuum permittivity. r and ϕ are the radial distance and angle in polar coordinates. The exact solutions of Equation (1) are [21]

$$E_n = -\frac{m_e e^4}{8\pi^2\varepsilon_0^2\hbar^2(2n-1)^2}, \tag{2}$$

and

$$\Psi_{nm}(r,\phi) = \Phi_m^0(\phi)R_{nm}(r) \tag{3}$$

where $\Phi_m^0 = e^{im\phi}$ is the azimuthal part and R_{nm} is the radial part of the 2D hydrogen wavefunctions. n and m are the principal quantum number and magnetic quantum number. Because the Hamiltonian and the momentum operator $\hat{L}_z$ commute each other, they have common eigenfunctions. As a result, $e^{im\phi}$, the eigenfunction of $\hat{L}_z$, is conventionally chosen to be the azimuthal wavefunction, as discussed in many papers [37–39].

We first explore this problem by solving the Schrödinger equation numerically using the 2D finite difference method [4,40]. Here, the xy-plane is divided into a uniform squared grid with a representing grid spacing. The positive charge of the nucleus is positioned at the origin, which is at the center of the plane, as seen in Figure S1 in the Supplementary Materials. Equation (1) can be rewritten in Cartesian coordinates using $\nabla^2 = \frac{\partial^2}{\partial x^2} + \frac{\partial^2}{\partial y^2}$ and $r^2 = x^2 + y^2$, and expressed in discretized form as

$$-\left[\frac{\left(\Psi_{i-1,j} - 2\Psi_{i,j} + \Psi_{i+1,j}\right)}{\tilde{a}^2} + \frac{\left(\Psi_{i,j-1} - 2\Psi_{i,j} + \Psi_{i,j+1}\right)}{\tilde{a}^2}\right] - \frac{2}{\sqrt{\tilde{x}^2 + \tilde{y}^2}}\Psi_{i,j} = \frac{E}{E_0}\Psi_{i,j}. \tag{4}$$

Here, $\Psi_{i,j}$ is the wavefunction at the position (i, j) in the xy-plane; $\widetilde{a} = a/a_0$, $\widetilde{x} = x/a_0$, $\widetilde{y} = y/a_0$, and $E_0 = \hbar^2/2m_e a_0^2$, where a_0 is the Bohr radius defined by $a_0 = 4\pi\varepsilon_0\hbar^2/m_e e^2$. The matrix eigenvalue problem corresponding to Equation (4) is shown in Note S1 in the Supplementary Materials and can be solved numerically to obtain the eigenenergies E and eigenstates Ψ.

In the next section, it will be demonstrated that the probability densities $|\Psi_{nm}|^2$ due to the numerical method differ from those due to the analytical conventional calculation. To confirm the numerical results, the new derivation is presented here to obtain the alternative expression of azimuthal wavefunctions. Unlike previous studies, our proposed eigenfunctions originate from the commutation of the Hamiltonian with the square of the angular momentum $\hat{L}_z^2 = -\hbar^2 \frac{\partial^2}{\partial\phi^2}$, whose eigenvalue problem is $-\hbar^2 \frac{\partial^2 \Phi}{\partial\phi^2} = (m\hbar)^2 \Phi$. This is the second-order differential equation with constant coefficients, and its solution is

$$\Phi_m(\phi) = C_m \cos(m\phi) + D_m \sin(m\phi) \tag{5}$$

where C_m and D_m are constants. Notice that our proposed Φ_m in Equation (5) is generally not the eigenfunction of $\hat{L}_z$, but the conventional Φ_m^0 in Equation (3) is the eigenfunction of $\hat{L}_z^2$. Therefore, the commutation relation between $\hat{L}_z$ and $\hat{L}_z^2$ ($[\hat{L}_z, \hat{L}_z^2] = 0$) can be represented by the Venn diagram in Figure 1. Note that the eigenfunctions of $\hat{L}_z^2$ in the blue region are concentrated and explored in this study.

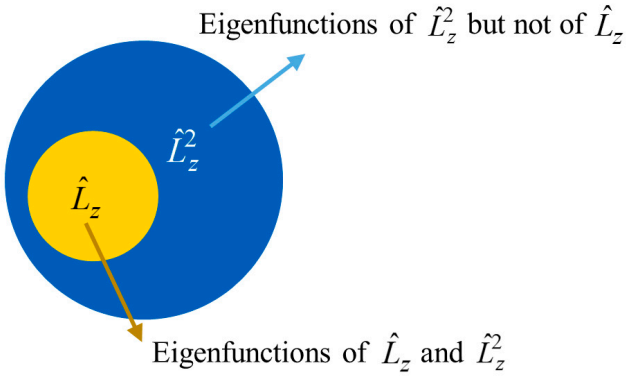

Figure 1. The Venn diagram of the eigenfunctions of $\hat{L}_z$ and $\hat{L}_z^2$.

The values of C_m and D_m in Equation (5) are determined from the normalization condition $\int_0^{2\pi} \Phi_m^* \Phi_m d\phi = 1$. It can be straightforwardly calculated that $C_{m=0} = \frac{1}{\sqrt{2\pi}}$ for the states with $m = 0$ and

$$C_m^2 + D_m^2 = \frac{1}{\pi} \tag{6}$$

for the states with $m \neq 0$. Additionally, the values of the coefficients C_m and D_m are determined from the orthogonality of the eigenstates. To achieve the orthogonal set of eigenstates, it is shown in Appendix A that the state with momentum m ($\Phi_m = C_m \cos(m\phi) + D_m \sin(m\phi)$) and the state with momentum $-m$ ($\Phi_{-m} = C_{-m} \cos(m\phi) - D_{-m} \sin(m\phi)$) are orthogonal when the coefficients satisfy the following relation:

$$C_m C_{-m} = D_m D_{-m}. \tag{7}$$

However, any two states with different values of $|m|$ are orthogonal regardless of the values of the coefficients.

In short, our calculation shows that the conventional azimuthal function Φ_m^0 in Equation (3) can be replaced by Φ_m in Equation (5), where coefficients C_m and D_m must satisfy Equations (6) and (7), which are derived and presented here for the first time. It will be shown later that the possible values of these coefficients influence the physical properties

of the 2D hydrogen states, such as rotation, orbital orientation, and optical transitions. For illustrating orbital shapes, the values of the coefficients C_m and D_m can be chosen to be 0 and $1/\sqrt{\pi}$ to obtain the azimuthal functions in the form of

$$\Phi_m(\phi) = \begin{cases} \frac{1}{\sqrt{\pi}}\cos(m\phi) & \text{for} \quad m > 0 \\ \frac{1}{\sqrt{2\pi}} & \text{for} \quad m = 0 \\ \frac{1}{\sqrt{\pi}}\sin(m\phi) & \text{for} \quad m < 0. \end{cases} \tag{8}$$

It will be demonstrated that the 2D hydrogen eigenfunctions $\Psi_{nm} = \Phi_m R_{nm}$, where Φ_m is defined in Equation (8), are convenient for labeling s, p, d, and f orbitals in the next section.

3. Results and Discussion

Firstly, the solutions of the 2D hydrogen atom from the conventional analytical calculation shown in Equations (2) and (3) are compared with those from the numerical method. As shown in Table 1, the eigenenergies and the number of degenerate states in each energy level obtained from these two independent methods are in good agreement.

Table 1. Energy levels obtained from the analytical method and finite difference method, denoted by E_n^{exact} and E_n^{num}, respectively. Note that there are 3, 5, and 7 degenerate states for the level n = 2, 3, and 4.

n	E_n^{exact}/E_0	E_n^{num}/E_0	Error (%)
1	−4.00000	−3.97619	0.59525
2	−0.44444	−0.44442	0.00450
	−0.44444	−0.44442	0.00450
	−0.44444	−0.44149	0.66376
3	−0.16000	−0.15998	0.01250
	−0.16000	−0.15993	0.04375
	−0.16000	−0.15987	0.08125
	−0.16000	−0.15987	0.08125
	−0.16000	−0.15872	0.80000
4	−0.08160	−0.08164	0.04901
	−0.08160	−0.08164	0.04901
	−0.08160	−0.08164	0.03676
	−0.08160	−0.08164	0.03676
	−0.08160	−0.08164	0.03676
	−0.08160	−0.08163	0.03676
	−0.08160	−0.08163	0.94363

(Note that the numerical method used does not directly identify degenerate states. However, by comparing the nearly identical numerical eigenenergies with exact analytical energy levels, we inferred that these correspond to degenerate states, as shown in Table 1.) However, the distributions of PDs $\left(|\Psi_{nm}|^2\right)$ of the states with $m \neq 0$ are different as seen in Figures 2 and 3. Clearly, all of the conventional PDs in Figure 2 are independent of the azimuthal angle ϕ because $|\Psi_{nm}|^2$ results in the cancelation of the azimuthal eigenfunction $e^{im\phi}$. In contrast, numerical PDs of the states with $m \neq 0$ in Figure 3 oscillate along the azimuthal direction and exhibit rotational symmetry. It appears that higher n states show a greater diversity of orders of rotational symmetry. This indicates that the numerical wavefunctions lead to distinctive azimuthal behaviors and specific orders of rotational symmetry not present in the conventional wavefunctions. It should be noted that Equation

(1) can also be solved using the variable-separable method, which is likely to yield results for the azimuthally dependent PDs and rotational symmetry similar to those obtained using the 2D finite difference method.

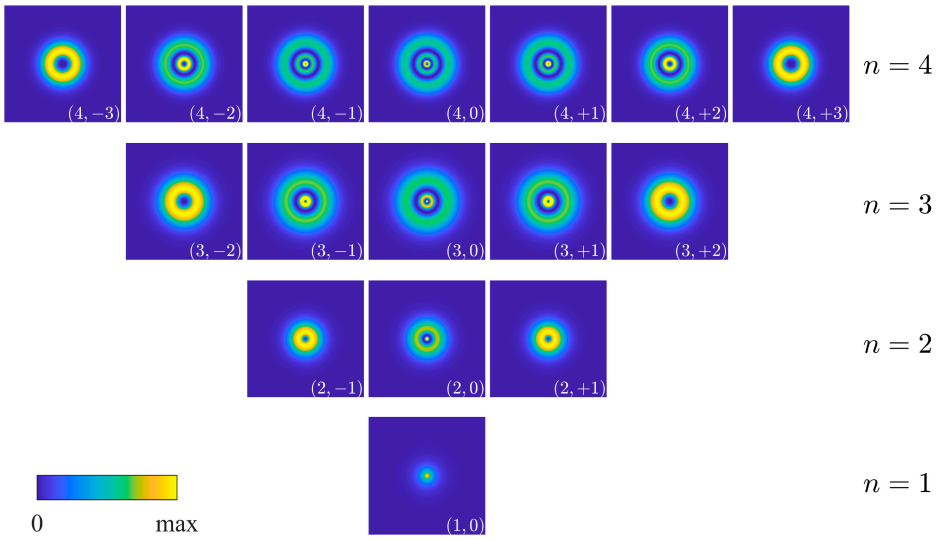

Figure 2. The distributions of PDs ($|\Psi|^2$) from the conventional calculation shown in Equation (3). (n, m) represent the quantum numbers of each state. The degenerate states are presented in the same lines and their corresponding energy levels (n) are shown on the right-hand side. PDs of the states with $n = 1, 2, 3$, and 4 are illustrated in squares with side lengths $5a_0$, $25a_0$, $45a_0$, and $95a_0$, respectively.

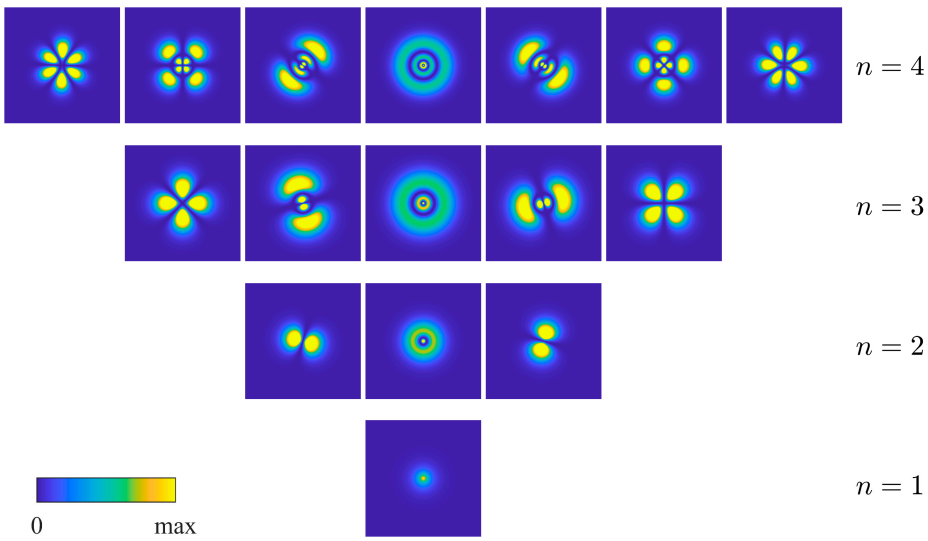

Figure 3. The distributions of PDs ($|\Psi|^2$) from the finite difference method. The degenerate states are presented in the same lines and their corresponding energy levels (n) are shown on the right-hand side. PDs of the states with $n = 1, 2, 3$, and 4 are illustrated in squares with side lengths $5a_0$, $25a_0$, $45a_0$, and $95a_0$, respectively.

To confirm the numerical results, the eigenfunctions Ψ due to the finite difference method are further investigated and compared with the analytical eigenfunctions Ψ_{nm} with our proposed Φ_m, defined in Equation (5). We find that oscillating along the azimuthal direction of the numerical eigenfunctions depends on the number of grid points determined by N (see Figure S1); several numerical eigenfunctions with $m \neq 0$ rotate unpredictably around the origin when the grid changes from N = 1500 to N = 2300, as seen in Figures S2–S5. For our analytic eigenfunctions Ψ_{nm}, the rotating behavior is also found when the values of C_m and D_m in Equation (5) are varied. To illustrate this behavior, we

have shown in Figure S6 that the eigenfunctions rotate clockwise when C_m increases or D_m decreases.

The eigenfunctions Ψ_{nm}, where the azimuthal part Φ_m is in the simple form as defined in Equation (8), are shown in Figure 4. One may notice that our analytical eigenfunctions in Figure 4 and the numerical eigenfunctions in Figures S2–S5 look very similar. To demonstrate that they are identical, the data of the numerical eigenfunctions $(\Psi_{i,j})$ are fitted to the analytic eigenfunctions by varying C_m and D_m to obtain the maximum values of the coefficient of determination (R^2). As seen in Table 2, $R^2 \geq 0.99$ for every eigenstate (n, m) indicates that our analytic eigenfunctions fit the numerical eigenfunctions extremely well. Moreover, the coefficients C_m and D_m of the state (n, m) and the state $(n, -m)$ in the table obey Equation (7). This means the numerical eigenstates (n, m) and $(n, -m)$ are orthogonal to each other. These agreements between our analytical and numerical solutions verify that the results of these two independent approaches are correct. In fact, the sinusoidal functions of azimuthal wavefunctions have been presented in a few papers [41,42]. However, the wavefunctions are not in a general form; the values of C_m and D_m are specified. Thus, their expression cannot be used to verify the correctness and rotating behavior of the numerical wavefunctions.

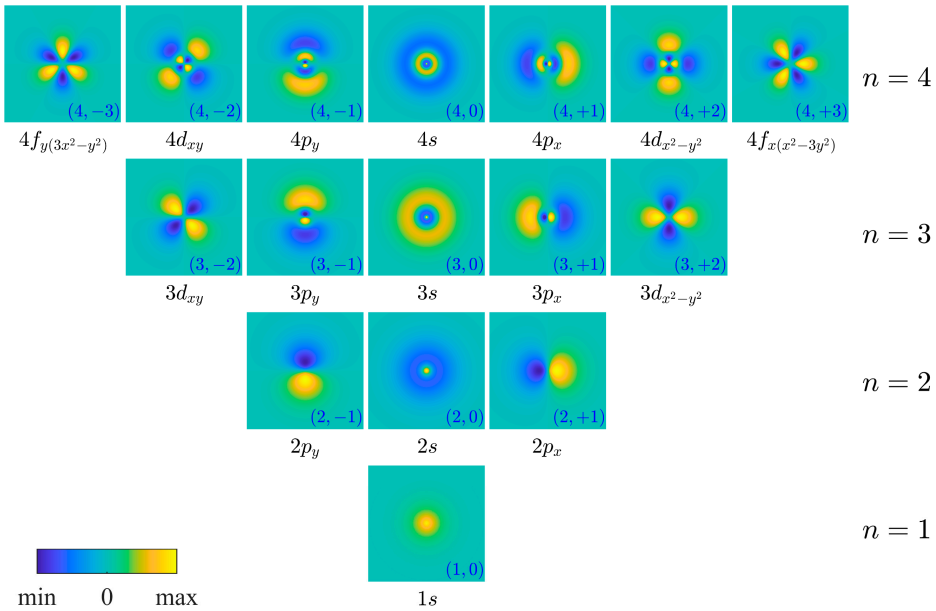

Figure 4. The eigenfunctions Ψ_{nm} with the azimuthal part Φ_m described in Equation (8). The degenerate states are presented in the same lines and their corresponding energy levels (n) are shown on the right-hand side. PDs of the states with $n = 1, 2, 3$, and 4 are illustrated in squares with side lengths $5a_0$, $25a_0$, $45a_0$, and $95a_0$, respectively. Cartesian representations of each orbital state are shown underneath each panel.

Next, the oscillator strength of our analytic eigenfunctions Ψ_{nm} is investigated and compared with that of the conventional eigenfunctions in Equation (3). This quantity indicates the probability of transition between states Ψ_{nm} and $\Psi_{n'm'}$, defined by $P_{nm}^{n'm'} = \frac{2m_e(E_{n'}-E_n)}{\hbar^2}\left|\int_0^{2\pi}\int_0^{\infty}\Psi_{n'm'}^{*}x\Psi_{nm}rdrd\phi\right|^2$ [43]. We first explore the transition from the ground state $(1, 0)$ to the first-excited degenerate states $(2, -1)$, $(2, 0)$, and $(2, 1)$. Similar to the transition of the conventional eigenfunctions, the possible transition between our eigenfunctions is found when $\Delta m = 1$. Therefore, P_{10}^{2-1} and P_{10}^{2+1} are presented in Figure 5. It is evident that they vary as a parabolic function with respect to C_m, which is further supported by the linear variation in the oscillator strengths, as shown in the inset where C_m^2 is varied. This relationship is also clearly derived from the definition of the oscillator strengths. Interestingly, although the values of $P_{10}^{2\pm1}$ due to our analytic eigenfunctions are determined by coefficients C_m and D_m, the summation of P_{10}^{2-1} and

P_{10}^{2+1} is constant with a value of 0.2109 (yellow line). This value is equal to the summation due to the conventional eigenfunctions. Note that for the conventional eigenfunctions, $P_{10}^{2-1} = P_{10}^{2+1} = 0.1055$. After investigating the oscillator strength between the ground state and the excited states in other energy levels, we also find agreement between the summation due to our eigenfunctions and due to the conventional eigenfunctions, as shown in Table 3. While the summations of the oscillator strengths for the traditional wavefunctions and ours are the same, the variation in individual oscillator strengths indicates that the transitions between energy states proceed through distinct pathways or exhibit different intensities, challenging further experiments.

Table 2. The values of R^2 obtained by fitting the proposed eigenfunctions due to Equation (5) to the numerical eigenfunctions corresponding to the PDs in Figure 3, using the given values of C_m and D_m.

Energy Level (n)	Numerical Eigenfunctions	Analytic Eigenfunctions (n,m)		C_m	D_m	R^2
1		(1,0)		$1/\sqrt{2\pi}$	0.0000	0.9997
2		(2,0)		$1/\sqrt{2\pi}$	0.0000	0.9998
		(2,+1)		−0.5407	0.1611	0.9999
		(2,−1)		−0.1611	0.5407	0.9999
3		(3,0)		$1/\sqrt{2\pi}$	0.0000	0.9989
		(3,+1)		0.5422	0.1560	0.9995
		(3,−1)		−0.1560	−0.5422	0.9995
		(3,+2)		−0.5642	0.0000	0.9998
		(3,−2)		0.0000	−0.5642	0.9999
4		(4,0)		$1/\sqrt{2\pi}$	0.0000	0.9981
		(4,+1)		0.4501	−0.3402	0.9904
		(4,−1)		−0.3402	0.4501	0.9904
		(4,+2)		−0.5642	0.0000	1.0000
		(4,−2)		0.0000	0.5642	1.0000
		(4,+3)		−0.5605	0.0644	0.9904
		(4,−3)		−0.0644	0.5605	0.9904

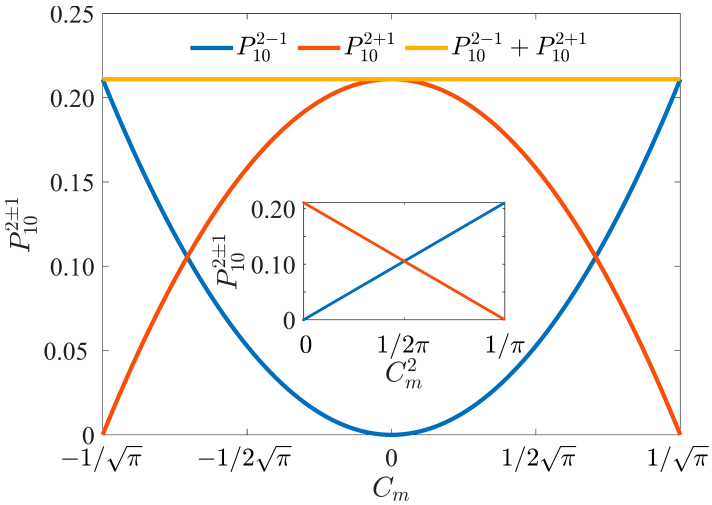

Figure 5. Variation in the oscillator strengths P_{10}^{2-1} and P_{10}^{2+1}, and their summation when C_m is varied. The inset shows the linear relationship between the oscillator strengths and C_m^2.

Table 3. Summation of the oscillator strengths $P_{10}^{n'-1}$ and $P_{10}^{n'+1}$ due to the conventional eigenfunctions and our proposed eigenfunctions for different values of n'.

Transition between States (1,0) and (n',±1)	$P_{10}^{n'-1}+P_{10}^{n'+1}$ **Due to the Conventional Eigenfunctions**	$P_{10}^{n'-1}+P_{10}^{n'+1}$ **Due to Our Proposed Eigenfunctions**
$(1,0) \to (2,\pm1)$	0.2109	0.2109
$(1,0) \to (3,\pm1)$	0.0381	0.0381
$(1,0) \to (4,\pm1)$	0.0132	0.0132

The advantage of our proposed wavefunctions is that they are appropriate for identifying orbital shapes labeled as s, p, d, and f, as well as for labeling the orientation of these shapes. Unlike the complex conventional wavefunctions, our 2D hydrogen wavefunctions are real-valued and clearly exhibit particular shapes, such as a circle, a ring, a dumbbell, and a cloverleaf, as seen in Figure 4. It should be noticed that these shapes look very similar to those in a 3D hydrogen atom [44]. For the 2D hydrogen atom, the azimuthal orbitals are characterized by their shapes and orientations, which are determined by the angular momentum quantum number m. The orbitals s, p, d, and f are labeled for the states with $m = 0,\ \pm1,\ \pm2,\ \pm3$, respectively, as seen in Figure 4. In a similar manner to a 3D hydrogen atom [45], the orientation of these orbitals can be labeled by transforming the azimuthal parts of the hydrogen wavefunctions into Cartesian coordinates on a circle with radius $r = 1$, as shown in Table 4. (The proof of this transformation can be found in Appendix B.) Labeling the orbitals by Cartesian representation provides the interpretation of the orbital orientations. For example, as seen in Figure 4, the maxima and minima of $p_x\,(p_y)$-orbital states align along the $x(y)$-axis. The maxima and minima of $d_{x^2-y^2}$-orbital states align along the x- and y-axes, while those of d_{xy}-orbital states align between the x- and y-axes. It should be noted that all Cartesian representations of 2D hydrogen states shown in Table 4 duplicate some of those in 3D hydrogen states, except for those with a z-coordinate, such as p_z, d_{xz}, d_{yz}, and f_{xyz}, which only appear in the 3D hydrogen states [46].

In short, illustrating 2D hydrogen wavefunctions using our expression reveals the intuitive characteristics of orbital shapes and their orientations. Here, the hydrogen states are labeled by Cartesian representations for the first time, whereas the angular momentum m was used in previous works [26,36,47]. Additionally, the azimuthal wavefunctions in Equation (5) can be applied to visualize the orbital characters of other quantum states confined in radial potentials, such as the Lennard-Jones potential [48] and the Woods–Saxon potential [49]. Our results, relevant to the concept of the optical transition between az-

imuthally dependent states, can also be applied to explain the transition in 2D systems with Coulomb potential, such as donor atoms and excitons in single-layer or thin materials [4–7].

Table 4. The azimuthal part for the 2D hydrogen states with angular momentum m and their Cartesian representation.

Angular Momentum	Azimuthal Wavefunctions	Cartesian Representation on a Circle with a Radius r=1	Orbitals with Labeling Orientation
$m = +1$	$\cos(\phi)$	x	p_x
$m = -1$	$\sin(\phi)$	y	p_y
$m = +2$	$\cos(2\phi)$	$x^2 - y^2$	$d_{x^2-y^2}$
$m = -2$	$\sin(2\phi)$	xy	d_{xy}
$m = +3$	$\cos(3\phi)$	$x(x^2 - 3y^2)$	$f_{x(x^2-3y^2)}$
$m = -3$	$\sin(3\phi)$	$y(3x^2 - y^2)$	$f_{y(3x^2-y^2)}$

4. Conclusions

In this study, we present alternative expressions of the azimuthal 2D hydrogen wavefunctions. Their probability densities corresponding to the states with $m \neq 0$ exhibit distinctive behavior; oscillating along the azimuthal direction is observed. This behavior is confirmed by the 2D finite difference method. After fitting the numerical wavefunctions to our proposed analytic wavefunctions, the values of R^2 are very close to one. Notably, although the summation of oscillator strengths from the ground state to excited degenerate states is identical for both the conventional and proposed wavefunctions, the wavefunction rotation causes a fundamental difference in optical mechanisms; the transitions between energy states happen through different pathways or with different intensities, suggesting new avenues for experimental verification and deeper understanding. Remarkably, the proposed wavefunctions are real-valued functions, providing an intuitive illustration of the orbital characteristics of the 2D hydrogen atom. Labeling the 2D hydrogen states using Cartesian representations suggests partial duplication in the orbital orientation between 2D and 3D hydrogen states. These results regarding orbital states provide a fundamental concept for describing science and technologies based on donor atoms and excitons in 2D materials.

Supplementary Materials: The following supporting information can be downloaded at https://www.mdpi.com/article/10.3390/sym16091163/s1: Note S1: The matrix eigenvalue problem; Figure S1: A square grid with side length S where wavefunctions are assumed to be zero at the edge grid points. $a = S/(N+1)$ is the distance between grid points, where $N+1$ is the number of the interval and the number of grid points is $(N+2)^2$; Figures S2–S5: The eigenfunctions Ψ from the finite difference method when using the grid with N = 1500 − 2300. The degenerate states are presented in the same lines and their corresponding energy levels (n) are shown on the right-hand side. PDs of the states with n =1, 2, 3, and 4 are illustrated in squares with side lengths $5a_0$, $25a_0$, $45a_0$, and $95a_0$, respectively; Figure S6: Examples of analytic eigenfunctions Ψ_{nm} from Equation (5), rotating around the origin when the coefficients C_m and D_m are varied and shown on the top of each column. Note that the coefficients must satisfy Equations (6) and (7).

Author Contributions: Conceptualization, A.A.; Methodology, A.A.; Software, P.S.; Validation, P.S. and A.A.; Formal Analysis, A.A.; Investigation, P.S. and S.J.; Data Curation, P.S. and S.J.; Visualization, P.S.; Writing—Original Draft, A.A.; Writing—Review and Editing, P.S., S.J. and A.A.; Supervision, A.A.; Project Administration, A.A.; Funding Acquisition, A.A. All authors have read and agreed to the published version of the manuscript.

Funding: This research was funded by the Faculty of Science at Naresuan University, grant number R2567E_SCI025.

Data Availability Statement: Data are contained within the article and Supplementary Materials.

Acknowledgments: We gratefully acknowledge the financial support for this work provided by the Faculty of Science at Naresuan University.

Conflicts of Interest: The authors declare no conflict of interest.

Appendix A. Orthogonality of Azimuthal Wavefunctions

The orthogonal relation between the azimuthal functions Φ_m and $\Phi_{m'}$ where $m \neq m'$, is described by the following equations:

$$\begin{aligned} 0 &= \int_0^{2\pi} \Phi_m \Phi_{m'} d\phi \\ &= \int_0^{2\pi} [C_m \cos(m\phi) + D_m \sin(m\phi)] \cdot [C_{m'} \cos(m'\phi) + D_{m'} \sin(m'\phi)] d\phi \\ &= (C_m C_{m'} + C_m D_{m'} + C_{m'} D_m + D_m D_{m'}) \cdot \left(\frac{0}{m^2 - m'^2} \right). \end{aligned}$$

That means if $m^2 \neq m'^2$ or $|m| \neq |m'|$, these states are orthogonal regardless of the values of the coefficients $C_m, D_m, C_{m'}$, and $D_{m'}$. However, $m^2 = m'^2$ leads to a denominator equal to zero. To solve this, the azimuthal functions Φ_m and $\Phi_{m'=-m}$ are considered, establishing the following orthogonal condition:

$$\begin{aligned} 0 &= \int_0^{2\pi} \Phi_m \Phi_{-m} d\phi \\ &= \int_0^{2\pi} [C_m \cos(m\phi) + D_m \sin(m\phi)] \cdot [C_{-m} \cos(m\phi) - D_{-m} \sin(m\phi)] d\phi \\ &= C_m C_{-m} \pi - D_m D_{-m} \pi. \end{aligned}$$

Therefore,

$$C_m C_{-m} = D_m D_{-m}.$$

That means if $m' = -m$ or $m^2 = m'^2$, the azimuthal functions Φ_m and Φ_{-m} are orthogonal when the coefficients $C_m,\ D_m,\ C_{m'}$, and $D_{m'}$ satisfy the above equation.

Appendix B. Proof of Cartesian Representation of Azimuthal Wavefunctions

For the states $m = \pm 1, \pm 2, \pm 3$, the azimuthal parts of the 2D hydrogen wavefunctions from Equation (8) on a circle with a radius $r = 1$ are given by

Case $m = 1$

$$\Phi_{m=1} = \cos(\phi) = \frac{r\cos(\phi)}{r} = \frac{x}{r}. \text{ At } r = 1 \Phi_{m=1} = x.$$

Case $m = -1$

$$\Phi_{m=-1} = \sin(\phi) = \frac{r\sin(\phi)}{r} = \frac{y}{r}. \text{ At } r = 1 \Phi_{m=-1} = y.$$

Case $m = 2$

$$\begin{aligned} \Phi_{m=2} &= \cos(2\phi) = \tfrac{r^2\cos(2\phi)}{r^2} = \tfrac{r^2\left(1-2\sin^2(\phi)\right)}{r^2} = \tfrac{1}{r^2}\left(r^2 - 2r^2\sin^2(\phi)\right) \\ &= \tfrac{1}{r^2}\left(r^2 - 2y^2\right) = \tfrac{1}{r^2}\left(x^2 + y^2 - 2y^2\right) = \tfrac{1}{r^2}\left(x^2 - y^2\right) = x^2 - y^2 \text{ at } r = 1. \end{aligned}$$

Case $m = -2$

$$\begin{aligned} \Phi_{m=-2} &= \sin(2\phi) = \tfrac{r^2\sin(2\phi)}{r^2} = \tfrac{r^2}{r^2} 2\sin(\phi)\cos(\phi) = \tfrac{2}{r^2} r\sin(\phi) r\cos(\phi) \\ &= \tfrac{2}{r^2} xy \propto xy \text{ at } r = 1. \end{aligned}$$

Case $m = 3$

$$\begin{aligned} \Phi_{m=3} &= \cos(3\phi) = \tfrac{r^3\cos(3\phi)}{r^3} = \tfrac{r^3\left(4\cos^3(\phi) - 3\cos(\phi)\right)}{r^3} = \tfrac{r\cos(\phi)\left(4r^2\cos^2(\phi) - 3r^2\right)}{r^3} \\ &= \tfrac{x\left(4x^2 - 3r^2\right)}{r^3} = \tfrac{x\left(4x^2 - 3x^2 - 3y^2\right)}{r^3} = \tfrac{x\left(x^2 - 3y^2\right)}{r^3} = x\left(x^2 - 3y^2\right) \text{ at } r = 1. \end{aligned}$$

Case $m = -3$

$$\begin{aligned}\Phi_{m=-3} &= \sin(3\phi) = \frac{r^3\sin(3\phi)}{r^3} = \frac{r^3\left(3\sin(\phi)-4\sin^3(\phi)\right)}{r^3} = \frac{r\sin(\phi)\left(3r^2-4r^2\sin^2(\phi)\right)}{r^3} \\ &= \frac{y\left(3x^2+3y^2-4y^2\right)}{r^3} = \frac{y\left(3x^2-y^2\right)}{r^3} = y\left(3x^2-y^2\right) \text{ at } r = 1.\end{aligned}$$

References

1. Pal, A.; Zhang, S.; Chavan, T.; Agashiwala, K.; Yeh, C.-H.; Cao, W.; Banerjee, K. Quantum-Engineered Devices Based on 2D Materials for Next-Generation Information Processing and Storage. *Adv. Mater.* **2023**, *35*, 2109894. [CrossRef] [PubMed]
2. Lee, S.; Kang, J.-H. Light-induced edge-excitation of two-dimensional surface polaritons in atomically thin crystals. *Results Phys.* **2024**, *57*, 107400. [CrossRef]
3. Xue, L.; Ren, Y.; He, J.-R.; Zhao, Y.; Xu, S.-L.; Hu, Y.; Hua, C.-B. The mechanical and thermal parameters of two-dimensional hexagonal materials evaluated using elastic properties: Monolayer MoS_2 as an example. *Results Phys.* **2024**, *57*, 107418. [CrossRef]
4. Pramjorn, N.; Amthong, A. Donor binding energies in a curved two-dimensional electron system. *Appl. Surf. Sci.* **2020**, *508*, 145195. [CrossRef]
5. Chouef, S.; Mommadi, O.; Boussetta, R.; Hbibi, M.; El Moussaouy, A.; Şahin, M.; Falyouni, F.; Duque, C.A. Effects of surface curvature and electric field on electronic and optical properties of an off-center hydrogenic donor impurity in 2D nanostructures. *Eur. Phys. J. Plus* **2024**, *139*, 381. [CrossRef]
6. García Flórez, F.; Siebbeles, L.D.A.; Stoof, H.T.C. Effects of material thickness and surrounding dielectric medium on Coulomb interactions and two-dimensional excitons. *Phys. Rev. B* **2020**, *102*, 125303. [CrossRef]
7. Mora-Ramos, M.E.; Duque, C.A. The formation of indirect excitons in atomic layer doped systems. *Superlattices Microstruct.* **2015**, *87*, 32–37. [CrossRef]
8. Abadillo-Uriel, J.C.; Koiller, B.; Calderón, M.J. Two-dimensional semiconductors pave the way towards dopant-based quantum computing. *Beilstein J. Nanotechnol.* **2018**, *9*, 2668–2673. [CrossRef]
9. Becher, C.; Gao, W.; Kar, S.; Marciniak, C.D.; Monz, T.; Bartholomew, J.G.; Goldner, P.; Loh, H.; Marcellina, E.; Goh, K.E.J.; et al. 2023 roadmap for materials for quantum technologies. *Mater. Quantum Technol.* **2023**, *3*, 012501. [CrossRef]
10. Hollenberg, L.C.L.; Greentree, A.D.; Fowler, A.G.; Wellard, C.J. Two-dimensional architectures for donor-based quantum computing. *Phys. Rev. B* **2006**, *74*, 045311. [CrossRef]
11. Moraru, D.; Udhiarto, A.; Anwar, M.; Nowak, R.; Jablonski, R.; Hamid, E.; Tarido, J.C.; Mizuno, T.; Tabe, M. Atom devices based on single dopants in silicon nanostructures. *Nanoscale Res. Lett.* **2011**, *6*, 479. [CrossRef] [PubMed]
12. Yadav, P.; Arora, H.; Samanta, A. Nitrogen in silicon for room temperature single-electron tunneling devices. *Appl. Phys. Lett.* **2023**, *122*, 083502. [CrossRef]
13. Wang, X.; Wyrick, J.; Kashid, R.V.; Namboodiri, P.; Schmucker, S.W.; Murphy, A.; Stewart, M.D., Jr.; Silver, R.M. Atomic-scale control of tunneling in donor-based devices. *Commun. Phys.* **2020**, *3*, 82. [CrossRef]
14. Mueller, T.; Malic, E. Exciton physics and device application of two-dimensional transition metal dichalcogenide semiconductors. *npj 2D Mater. Appl. 2.1* **2018**, *2*, 29. [CrossRef]
15. Sharma, A.; Hasan, M.M.; Lu, Y. Exciton dynamics in 2D organic semiconductors. *Mater. Futures* **2022**, *1*, 042001. [CrossRef]
16. Xiao, J.; Zhao, M.; Wang, Y.; Zhang, X. Excitons in atomically thin 2D semiconductors and their applications. *Nanophotonics* **2017**, *6*, 1309–1328. [CrossRef]
17. Parfitt, D.G.W.; Portnoi, M.E. The two-dimensional hydrogen atom revisited. *J. Math. Phys.* **2002**, *43*, 4681–4691. [CrossRef]
18. Stephanovich, V.A. On the discreet spectrum of fractional quantum hydrogen atom in two dimensions. *Phys. Scr.* **2019**, *94*, 125108. [CrossRef]
19. Kirchbach, M.; Vallejo, J.A. Wave functions of the Hydrogen atom in the momentum representation. *J. Phys. A Math. Theor.* **2023**, *56*, 125302. [CrossRef]
20. Zaslow, B.; Zandler, M.E. Two-dimensional analog to the hydrogen atom. *Am. J. Phys.* **1967**, *35*, 1118–1119. [CrossRef]
21. Yang, X.L.; Guo, S.H.; Chan, F.T.; Wong, K.W.; Ching, W.Y. Analytic solution of a two-dimensional hydrogen atom. *I. Nonrelativ. Theory. Phys. Rev. A* **1991**, *43*, 1186.
22. Stevanović, L.; Sen, K.D. Simultaneous degeneracy of the confined 2D hydrogen atom energy levels. *J. Phys. B At. Mol. Opt. Phys.* **2008**, *41*, 205002. [CrossRef]
23. Aquino, N.; Campoy, G.; Flores-Riveros, A. Accurate energy eigenvalues and eigenfunctions for the two-dimensional confined hydrogen atom. *Int. J. Quantum Chem.* **2005**, *103*, 267–277. [CrossRef]
24. Chaos-Cador, L.; Ley-Koo, E. Two-dimensional hydrogen atom confined in circles, angles, and circular sectors. *Int. J. Quantum Chem.* **2005**, *103*, 369–387. [CrossRef]
25. Szmytkowski, R. Two-dimensional hydrogen-like atom in a weak magnetic field. *Eur. Phys. J. Plus* **2018**, *133*, 311. [CrossRef]
26. Le, D.-N.; Hoang, N.-T.D.; Le, V.-H. Exact analytical solutions of a two-dimensional hydrogen atom in a constant magnetic field. *J. Math. Phys.* **2017**, *58*, 042102. [CrossRef]
27. Szmytkowski, R. Second-order stark effect and polarizability of a relativistic two-dimensional hydrogenlike atom in the ground state. *Phys. Rev. A* **2018**, *98*, 042507. [CrossRef]
28. Pedersen, T.G.; Mera, H.; Nikolić, B.K. Stark effect in low-dimensional hydrogen. *Phys. Rev. A* **2016**, *93*, 013409. [CrossRef]

29. Robnik, M.; Romanovski, V.G. Two-dimensional hydrogen atom in a strong magnetic field. *J. Phys. A Math. Gen.* **2003**, *36*, 7923. [CrossRef]
30. Soylu, A.; Bayrak, O.; Boztosun, I. The energy eigenvalues of the two dimensional hydrogen atom in a magnetic field. *Int. J. Mod. Phys. E* **2006**, *15*, 1263–1271. [CrossRef]
31. Meleshenko, P.A.; Nguyen, H.T.T.; Klinskikh, A.F. Spectroscopic peculiarities in a 2D Coulomb potential under Aharonov-Bohm effect. *Eur. Phys. J. D* **2013**, *67*, 209. [CrossRef]
32. Koval, E.A.; Koval, O.A. Excited states of two-dimensional hydrogen atom in tilted magnetic field: Quantum chaos. *Phys. E Low-Dimens. Syst. Nanostruct.* **2017**, *93*, 160–166. [CrossRef]
33. Koval, E.A.; Koval, O.A. Anisotropic features of two-dimensional hydrogen atom in magnetic field. *J. Exp. Theor. Phys.* **2017**, *125*, 35–42. [CrossRef]
34. Xie, W. A study of a hydrogen atom in a two-dimensional quantum well. *Nucl. Instrum. Methods Phys. Res. Sect. B Beam Interact. Mater. At.* **2010**, *268*, 3321–3324. [CrossRef]
35. Grimaldi, C. Energy levels of a two-dimensional hydrogen atom with spin-orbit Rashba interaction. *Phys. Rev. B* **2008**, *77*, 113308. [CrossRef]
36. Poszwa, A. Two-dimensional hydrogen-like atom in magnetic field in the presence of Rashba spin–orbit coupling. *Phys. E Low-Dimens. Syst. Nanostruct.* **2020**, *124*, 114247. [CrossRef]
37. Szafran, B.; Adamowski, J.; Bednarek, S. Electron–electron correlation in quantum dots. *Phys. E Low-Dimens. Syst. Nanostruct.* **1999**, *5*, 185–195. [CrossRef]
38. Kormányos, A.; Zólyomi, V.; Drummond, N.D.; Burkard, G. Spin-orbit coupling, quantum dots, and qubits in monolayer transition metal dichalcogenides. *Phys. Rev. X* **2014**, *4*, 011034. [CrossRef]
39. Prabhakar, S.; Melnik, R.; Bonilla, L.L. Coupled multiphysics, barrier localization, and critical radius effects in embedded nanowire superlattices. *J. Appl. Phys.* **2013**, *113*, 244306. [CrossRef]
40. Joonhuay, J.; Sathongpaen, P.; Amthong, A. Structural design of triangular core–shell nanowires for sensing polarized mid-infrared light. *Mater. Des.* **2023**, *230*, 111983. [CrossRef]
41. Amore, P.; Fernández, F.M. Bound states for the quantum dipole moment in two dimensions. *J. Phys. B At. Mol. Opt. Phys.* **2012**, *45*, 235004. [CrossRef]
42. Dasbiswas, K.; Goswami, D.; Yoo, C.-D.; Dorsey, A.T. Bound states of edge dislocations: The quantum dipole problem in two dimensions. *Phys. Rev. B* **2010**, *81*, 064516. [CrossRef]
43. Thongnak, V.; Joonhuay, J.; Amthong, A. Polarization-selective absorption in an off-centered core-shell square quantum wire. *Opt. Lett.* **2021**, *46*, 3259–3262. [CrossRef]
44. Griffiths, D.J.; Schroeter, D.F. *Introduction to Quantum Mechanics*, 2nd ed.; Cambridge University Press: Cambridge, UK, 2018.
45. Ashkenazi, G. The meaning of d-orbital labels. *J. Chem. Educ.* **2005**, *82*, 323. [CrossRef]
46. Gil, V.M.S. *Orbitals in Chemistry: A Modern Guide for Students*; Cambridge University Press: Cambridge, UK, 2000.
47. Le, N.H.; Lanskii, G.V.; Aeppli, G.; Murdin, B.N. Giant non-linear susceptibility of hydrogenic donors in silicon and germanium. *Light Sci. Appl.* **2019**, *8*, 64. [CrossRef]
48. Acosta-Humánez, M.F.; Acosta-Humánez, P.B.; Tuirán, E. Generalized Lennard-Jones Potentials, SUSYQM and Differential Galois Theory. *SIGMA. Symmetry Integr. Geom. Methods Appl.* **2018**, *14*, 099. [CrossRef]
49. Badalov, V.H.; Ahmadov, H.I.; Ahmadov, A.I. Analytical solutions of the Schrödinger equation with the Woods–Saxon potential for arbitrary l state. *Int. J. Mod. Phys. E* **2009**, *18*, 631–641. [CrossRef]